J. Earth Syst. Sci. (2019) 128:167
https://doi.org/10.1007/s12040-019-1185-7

Pb isotope geochemistry of the late Miocene–Pliocene volcanic rocks from Todeshk, the central part of the Urumieh–Dokhtar magmatic arc, Iran: Evidence of an enriched mantle source

Mahnaz Khodami

Department of Geology, Yazd University, Yazd, Iran.
e-mail: Khodami_m@yazd.ac.ir

MS received 12 July 2018; revised 8 February 2019; accepted 19 March 2019; published online 17 June 2019

The late Miocene–Pliocene volcanic rocks from Todeshk, south-east of Isfahan, are located in the middle of the Urumieh–Dokhtar magmatic belt. The belt is considered the subduction-related magmatic arc. The late Miocene–Pliocene calc-alkaline volcanic rocks are mainly andesite and dacite. The rocks have been formed during the post-collisional stage of the Zagros orogen. Geochemical data show the enrichment of light rare-earth elements and large ion lithophile elements such as Cs, Rb, K, Pb, Ba and Th as well as the depletion of elements with high field strength such as Nb, Ta and Ti. The Pb–Sr–Nd isotopic ratios of the studied rocks are characterised by $^{206}Pb/^{204}Pb$ = 18.41–18.72; $^{207}Pb/^{204}Pb$ = 15.64–15.67; $^{208}Pb/^{204}Pb$ = 38.49–38.83; $^{207}Pb/^{206}Pb$ = 0.8372–0.8496; $^{208}Pb/^{206}Pb$ = 2.0743–2.0905; $^{87}Sr/^{86}Sr$ = 0.7051–0.7068 and $^{143}Nd/^{144}Nd$ = 0.5125. The rocks have $\Delta 7/4Pb$ = 15.44–15.82 and $\Delta 8/4Pb$ = 57.26–60.44. Based on petrological studies and the whole rock Pb, Sr and Nd isotopes data, the late Miocene–Pliocene calc-alkaline volcanic rocks have been generated from the partial melting of the subduction-related metasomatised mantle. Additionally, the slab-derived melts and fluids were recycled into the mantle source. The data demonstrate that terrigenous sediments accompanied by a subducted slab play an important role in the formation of the enriched mantle as the source of volcanic rocks.

Keywords. Pb isotopes geochemistry; calc-alkaline; enriched mantle; Urumieh–Dokhtar magmatic arc; Zagros orogen; Iran.

1. Introduction

The late Miocene–Pliocene volcanic rocks in Todeshk are significant constituents in the studied area. The volcanic rocks are situated in the middle of the Urumieh–Dokhtar magmatic arc (UDMA), about 120 km south-east of Isfahan (figure 1a). The UDMA is a large magmatic belt in the Zagros orogen, which is the result of the opening and closure of the Neo-Tethys Ocean (Alavi 1980, 2004; Omrani *et al.* 2008; Davoudian *et al.* 2016). The Zagros orogen is a part of the Alpine–Himalayan orogenic belt and consists of parallel tectonic subdivisions from the south-west to the north-east: (i) The Zagros simply folded belt and the main Zagros thrust, which is suggested to be the suture zone between Gondwana and Eurasia; (ii) the Sanandaj–Sirjan zone which

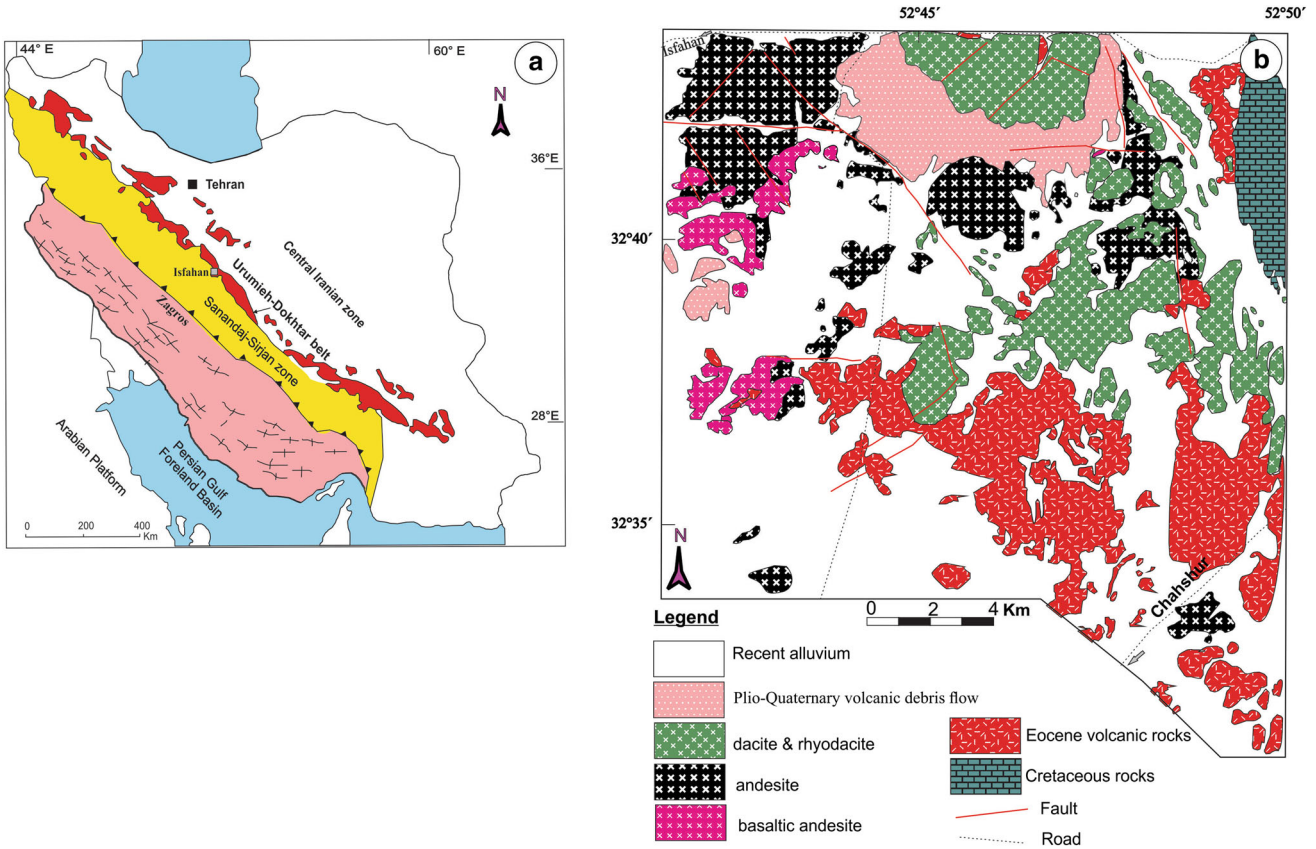

Figure 1. (**a**) Position of the studied area in the structural units of Iran (Mohajjel *et al.* 2003) and (**b**) the geological map of the studied area (simplified from the geological map of 1:250,000 Nain, Nabavi and Amidi 1978).

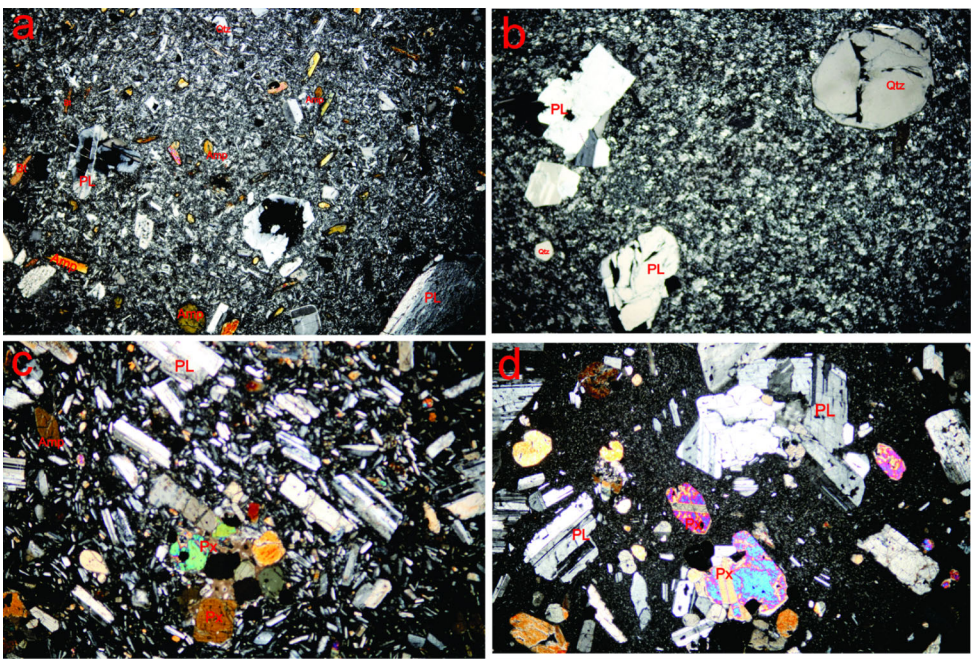

Figure 2. Representative photomicrographs for dacites (**a**) consisting of plagioclase phenocrysts and microphenocrysts of amphibole, biotite, quartz and (**b**) quartz and plagioclase in felsitic groundmass (CPL, field of view 4 mm), representative photomicrographs of andesites, (**c**) comprising plagioclase, pyroxene and amphibole with a glomeroporphyritic texture and (**d**) comprising plagioclase and pyroxene with a porphyritic texture (CPL, field of view 4 mm). Bi = biotite, Amp = amphibole, Px = pyroxene, Pl = plagioclase, and Qz = quartz.

Table 1. *Whole-rock isotopic data of volcanic rocks.*

Sample	AR2 Andesite	DH7 Dacite	OG4 Dacite	RS2 Dacite	TO4 Andesite
$^{207}Pb/^{206}Pb$	0.849556	0.844521	0.84897	0.837225	0.846509
2σ	0.00001	0.00001	0.00001	0.00001	0.00001
$^{208}Pb/^{206}Pb$	2.090523	2.084596	2.089768	2.074348	2.0850746
2σ	0.00003	0.00004	0.00003	0.00003	0.00003
$^{207}Pb/^{204}Pb$	15.64101	15.65614	15.64264	15.67378	15.65264
2σ	0.00087	0.00077	0.00077	0.00079	0.00063
$^{208}Pb/^{204}Pb$	38.48755	38.64418	38.50355	38.83326	38.56566
2σ	0.00222	0.00204	0.00190	0.00202	0.00142
$^{206}Pb/^{204}Pb$	18.410571	18.53825	18.42523	18.72091	18.49061
2σ	0.00096	0.00075	0.00081	0.00081	0.00061
$^{87}Sr/^{86}Sr$	0.705096	0.705925	0.706396	0.706096	0.706792
2σ	0.000031	0.000022	0.000021	0.000017	0.000082
$^{143}Nd/^{144}Nd$	nd	0.512525	nd	0.512552	nd
2σ		0.00002		0.00001	
$\Delta 7/4Pb^*$	15.5210	15.6591	15.5331	15.4432	15.8255
$\Delta 8/4Pb^{**}$	60.2178	60.444	60.0344	57.2675	58.3519

$^*\Delta 7/4Pb = 100\,9\,[(^{207}Pb/^{204}Pb) - 0.1084\,9\,(^{206}Pb/^{204}Pb) - 13.491]$ (Hart 1984). nd: not detected.
$^{**}\Delta 8/4Pb = 100\,9\,[(^{208}Pb/^{204}Pb) - 1.209\,9\,(^{206}Pb/^{204}Pb) - 15.627]$.

is the internal part of the Zagros orogen consisting of metamorphic complexes and igneous plutons (Stöcklin 1968; Davoudian *et al.* 2016) and (iii) the UDMA, which is a subduction-related magmatic arc along the active margin of the Iranian plate (Berberian and Berberian 1981; Alavi 1994, 2004; Omrani *et al.* 2008). Magmatic activity in the UDMA created a wide belt of mostly Cenozoic volcanic and plutonic rocks. The UDMA is located between the Sanandaj–Sirjan zone and the Central Iran structural zone (figure 1a) (Berberian and Berberian 1981; Mohajjel *et al.* 2003). The maximum magmatic activity in the UMDA occurred in the Eocene period, but after a period of inactivity, has continued during the upper Miocene to the Plio-Quaternary (Omrani *et al.* 2008). However, the studies indicate that a collision occurred in the Oligocene–late Miocene, and although the active subduction between the Iranian edge of Eurasia and the Arabian plate as a part of Gondwana had ended, the magmatic activity did not stop (Berberian and Berberian 1981; Hassanzadeh 1993; Ghasemi and Talbot 2005; Omrani *et al.* 2008). The late Miocene to the Plio-Quaternary volcanism in the UDMA belongs to the post-collision magmatic activity which is probably the result of a break off the Neo-Tethys slab (Omrani *et al.* 2008). Magmatism in a subduction-related setting originates from the partial melting of the mantle wedge, lower crust, oceanic slab, slab

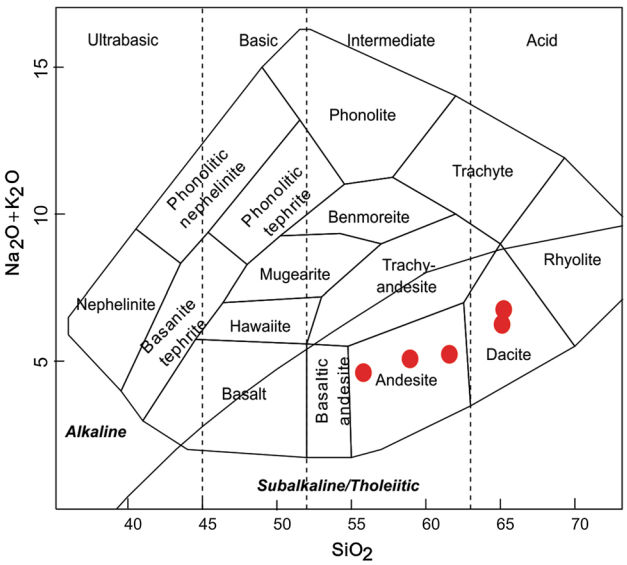

Figure 3. Classification of the volcanic rocks in the TAS diagram (Cox *et al.* 1979; data from Khodami *et al.* 2010).

sediments or releasing of fluids by the dehydration of the subducting oceanic slab (Tatsumi and Takahashi 2006). Pb isotope data can demonstrate the origin and proportion of involvement of mantle, slab, sediments or continental crust in the generation of parental magma. ^{204}Pb is non-radiogenic, while $^{208}Pb/^{204}Pb$, $^{207}Pb/^{204}Pb$ and $^{206}Pb/^{204}Pb$ increase during U and Th decays (Faure 1986). The most important mantle sources are identified by isotopic features as depleted mid-ocean ridge

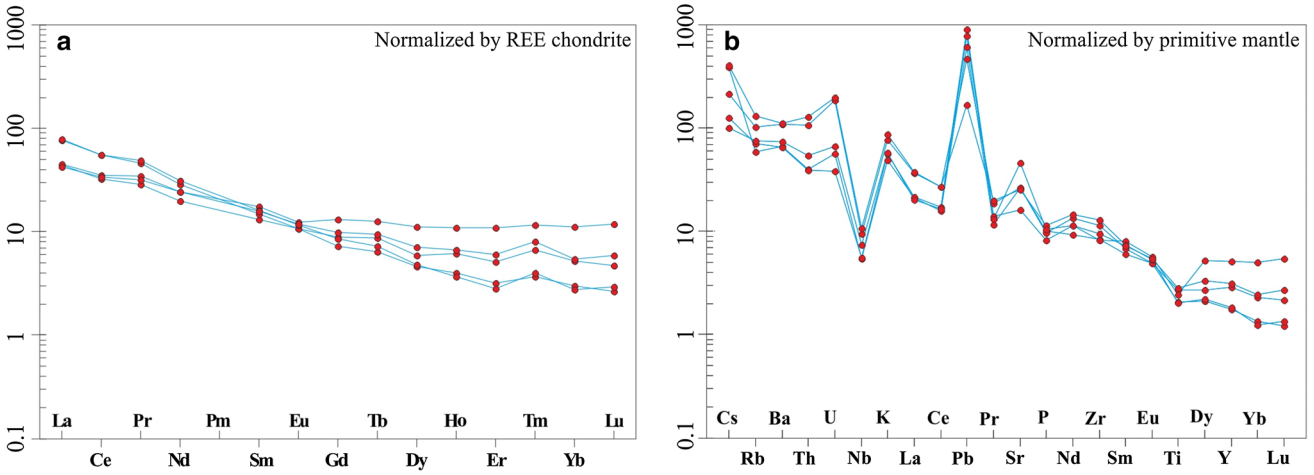

Figure 4. (**a**) Chondrite-normalised REE element patterns of volcanic rocks (chondrite-normalising values are from Nakamura (1974). (**b**) Primitive mantle-normalised patterns of volcanic rocks. Normalising values are from Sun and Mcdonough (1989) (data from Khodami *et al.* 2010).

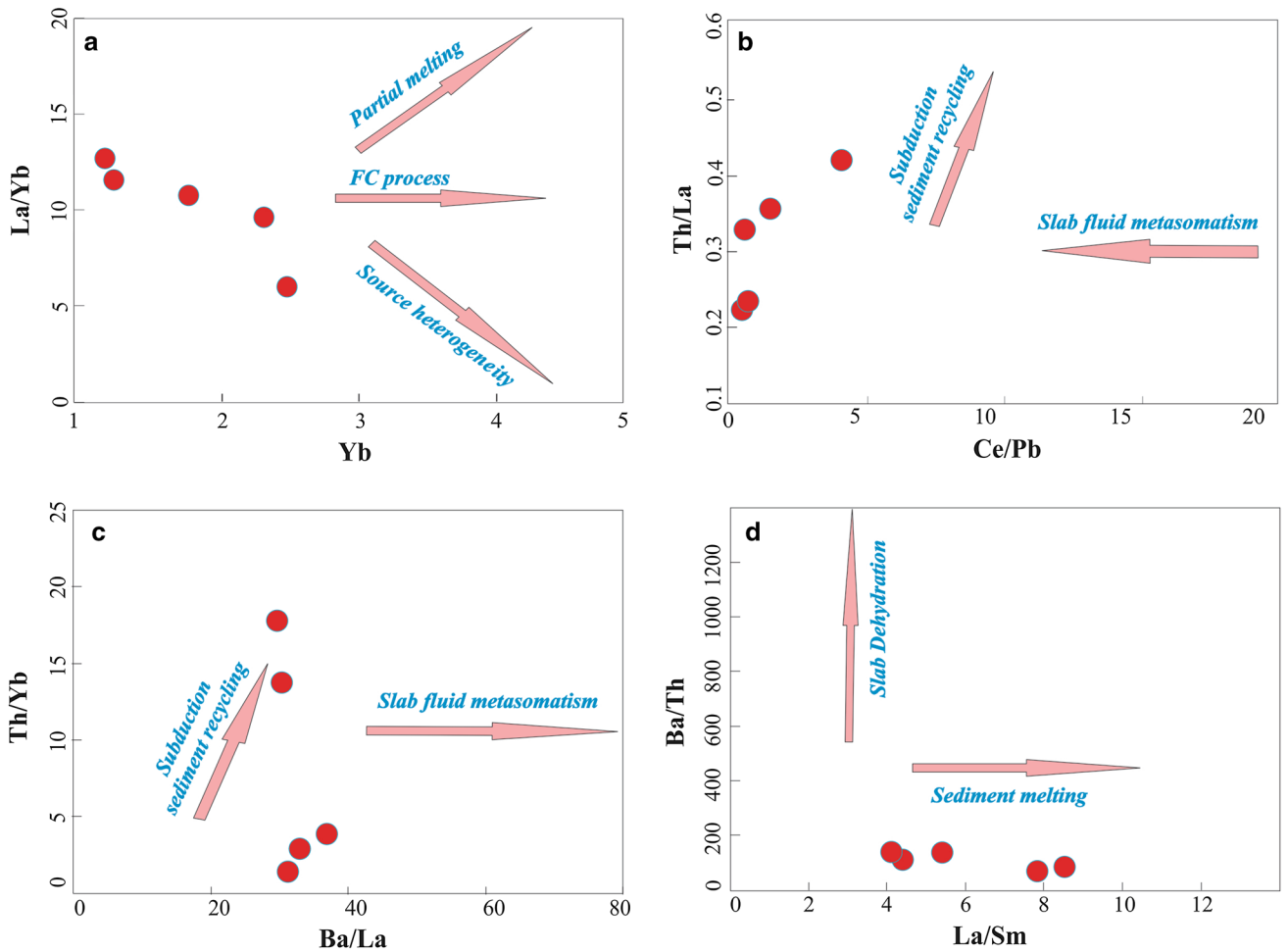

Figure 5. (**a**) La/Yb *vs.* Yb diagram, (**b**) Th /La *vs.* Ce/Pb diagram, (**c**) Th/Yb *vs.* Ba/La diagram and (**d**) Ba/Th *vs.* La/Sm diagram of volcanic rocks (Wang *et al.* 2006; Arslan *et al.* 2013; Qian *et al.* 2016; data from Khodami *et al.* 2010).

basalts (MORBs) or the depleted MORB mantle (DMM), high mu, mu = $^{238}U/^{204}Pb$ (HIMU), enriched mantle type I (EMI) and enriched mantle type II (EMII) (Faure 1986; Zindler and Hart 1986). The HIMU sources were generated when the subducted oceanic crust was dehydrated and

remained in the deep mantle for a long period. The HIMU have high U/Pb, Th/Pb and Sr/Rb ratios and indicate the radiogenic evolution of ^{206}Pb and ^{207}Pb (Wilson 1989). The DMM reservoirs have a U-depleted composition. The EMI has a geochemical composition similar to the lower crust or marine pelagic sediments as reported from carbonatite metasomatism in the lithospheric mantle (White 2003; Lustrino and Anderson 2015). The EMI sources have high Th/U and low U, Th/Pb ratios, negative anomalies of Hf, Zr and positive anomalies of Eu. EMI can be formed by recycling the lower continental crust or subducted pelagic sediments (White 2003; Lustrino and Anderson 2015; Yamgouot *et al.* 2016). The EMII mantle end-member is characterised by the $^{206}Pb/^{204}Pb$ intermediate between EMI and HIMU, a relatively high $^{207}Pb/^{204}Pb$ ratio (for a given $^{206}Pb/^{204}Pb$), negative anomalies of Nb, Ta and the lack of positive anomalies of Eu. The EMII has been reported from subduction environments and perhaps modified by recycling the oceanic crust and subducted terrigenous sediments. The $^{87}Sr/^{86}Sr$ ratios of EMI–EMII are higher than DMM and bulk silicate earth or the primary uniform reservoir (White 2003; Workman *et al.* 2004; Lustrino and Anderson 2015; Yamgouot *et al.* 2016). Generally, the elements Pb, Th and U are concentrated in the continental crust, and the Pb isotopic composition of the mantle is sensitive to the crustal components. Therefore, the isotopic compositions of HIMU, EMI and EMII are mainly related to recycling subducted lithologies such as the oceanic crust, pelagic or terrigenous sediments and the lower continental crust. In the absence of oxygen isotopic data, we have applied the new whole rock Pb, Sr and Nd isotopic ratios together with major and trace elements to determine the magmatic source of the late Miocene–Pliocene volcanic rocks in Todeshk, in the south-east of Isfahan as a central part of UDMA.

2. Geological setting

The late Miocene–Pliocene volcanic rocks in the UDMA outcrop in the south-east and north-west of Isfahan with a NW–SE trend. The studied area is located 130-km south-east of Isfahan and near Todeshk. The Cretaceous units are also observable in the north of the area, consisting of limestone and slightly metamorphosed volcanic rocks. However, most of the magmatic activity occurred in the Eocene, including varieties of the volcanic and the volcano-sedimentary rocks. Miocene reddish-grey conglomerate and sandstone as Red formation are the other lithological units (Nabavi and Amidi 1978). The andesitic lava flows across the Upper Red formation. The dacitic domes and lava domes intruded into the andesite and probably they belong to the latest volcanic activity in the area (figure 1b) (Nabavi and Amidi 1978). Based on stratigraphy, the volcanic rocks were emplaced during the late Miocene–Pliocene after the collision between the Iranian and Arabian platforms. One available K–Ar age dating for a dacitic dome has exhibited 14.1 ± 0.8 Ma (Ghorbani *et al.* 2014). The dacites consist of plagioclase and various amounts of orthopyroxene, amphibole, biotite, quartz and opaque oxides, set in a colourless to pale brown glass or felsitic groundmass (figure 2a and b). The andesites contain abundant phenocrysts of plagioclase, pyroxene or amphibole, biotite and opaque oxides, set in a brown glass matrix with microlites of plagioclase and microphenocrysts of pyroxene or

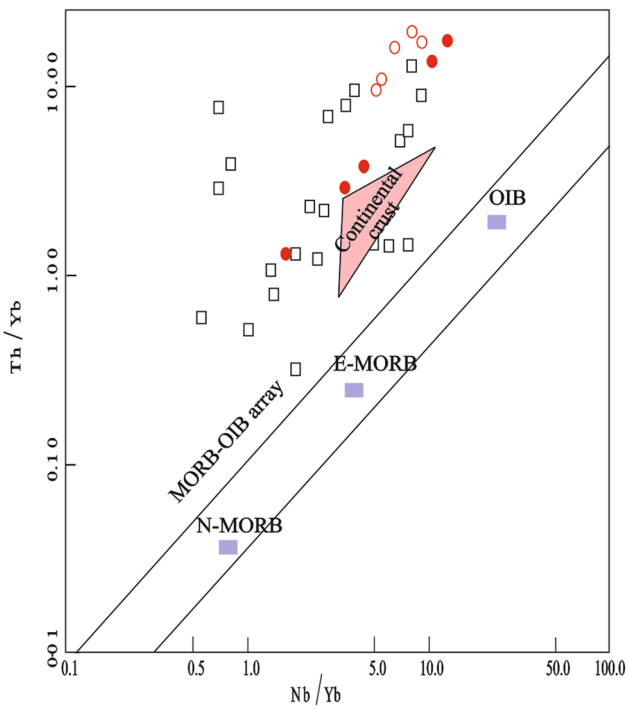

Figure 6. Th/Yb *vs.* Nb/Yb diagram (Pearce (2008), N-MORB, E-MORB, OIB are from Sun and Mcdonough (1989), average continental crust is from Rudnick and Fountain (1995) and subducted sediment trench averages are from Plank and Langmuir (1998)). (White box subducted sediment, red circles (table 1) and white circles are from the north-west of Isfahan, data from Khodami 2011).

amphibole (figure 2c and d). The most abundant mineral is plagioclase, and its textures are mainly porphyritic.

3. Materials and methods

The Sr, Nd and Pb isotopic ratios of five samples of the volcanic rocks are presented in table 1. For the Sr–Nd–Pb isotopic determination, the late Miocene–Pliocene volcanic rocks were analysed using the multi-collector ICP-MS (Nu Plasma) at the State Key Laboratory of Continental Dynamics, Northwest University, China. Also, the available isotopic data of the late Miocene–Pliocene volcanic rocks from the north-west of Isfahan are considered to make a conclusion (Khodami 2011). The Sr and Nd isotopic ratios were corrected for mass fractionation relative to $^{86}Sr/^{88}Sr = 0.1194$ and $^{146}Nd/^{144}Nd = 0.7219$, respectively. The BCR-2 standard yielded an $^{87}Sr/^{86}Sr$ ratio of 0.704959 ± 36 and $^{143}Nd/^{144}Nd$ ratio of 0.512613 ± 19, compared with its reported $^{87}Sr/^{86}Sr$ ratio of 0.704958 and $^{143}Nd/^{144}Nd$ ratio of 0.512633. Pb isotopic fractionation was normalised to $^{205}Tl/^{203}Tl = 2.3875$. Within the analytical period, measurements of NBS SRM981 gave average values of $^{206}Pb/^{204}Pb = 16.942 \pm 0.0014(2\sigma)$, $^{207}Pb/^{204}Pb = 15.495 \pm 0.0014$ and $^{208}Pb/^{204}Pb = 36.716 \pm 0.0032$. BCR-2 standard gave $^{206}Pb/^{204}Pb = 18.735 \pm 0.0009(2\sigma)$, $^{207}Pb/^{204}Pb = 15.621 \pm 0.0008$ and $^{208}Pb/^{204}Pb = 38.684 \pm 0.0020$.

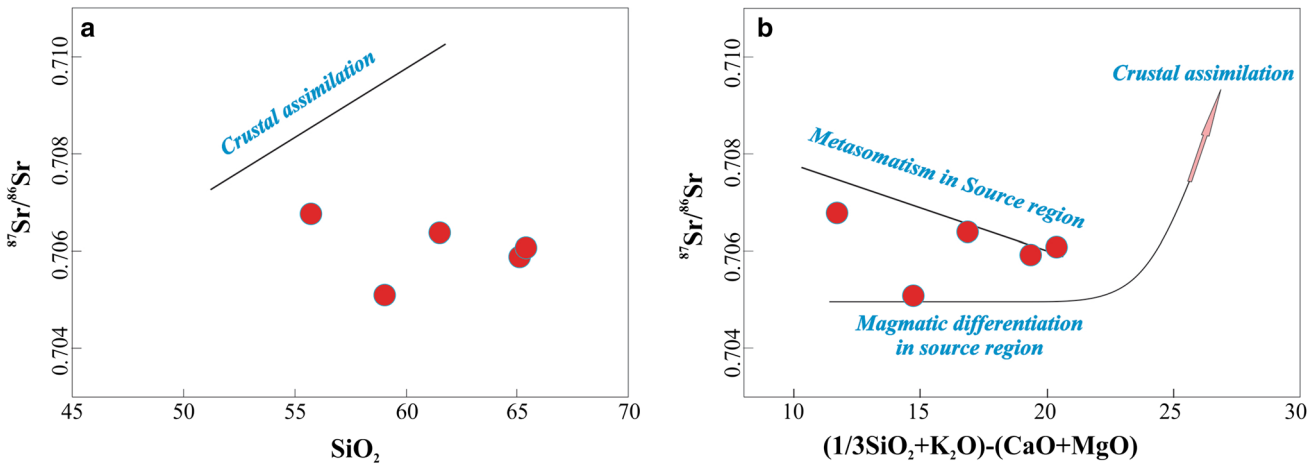

Figure 7. (**a**) Sr isotope ratios *vs.* SiO_2 and (**b**) MDI = (1/3 $SiO_2 + K_2O$)–($CaO + MgO$) diagrams (Wang *et al.* 2006; Arslan *et al.* 2013; data from Khodami *et al.* 2010).

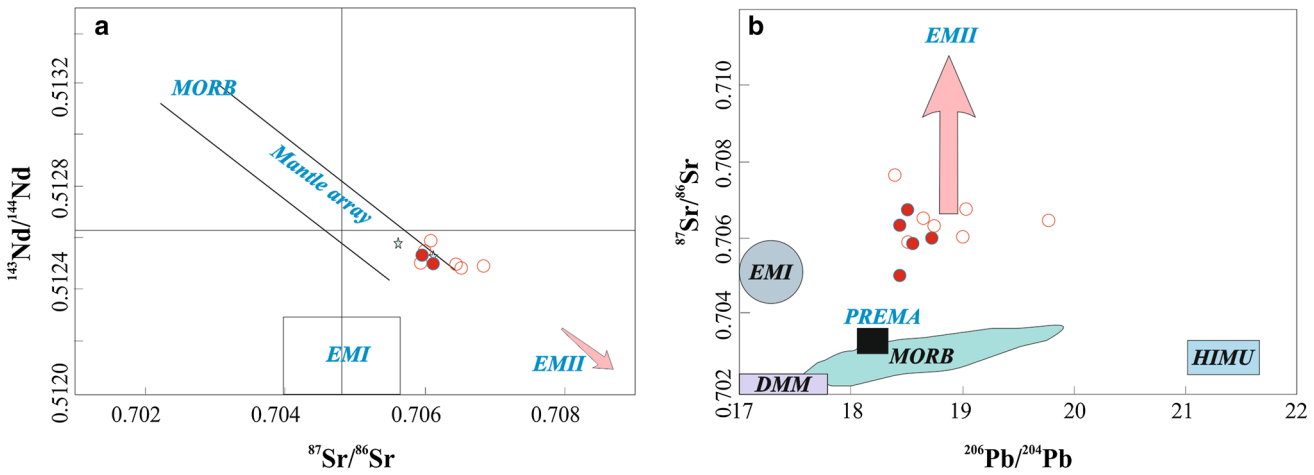

Figure 8. Plots of Sr–Nd–Pb isotopic ratios for the volcanic rocks: (**a**) $^{87}Sr/^{86}Sr$ *vs.* $^{143}Nd/^{144}Nd$ diagram, (**b**) $^{87}Sr/^{86}Sr$ *vs.* $^{206}Pb/^{204}Pb$ diagram; mantle components including depleted mantle (DM), enriched mantle I (EMI), enriched mantle II (EMII), high U/Pb mantle (HIMU) are from Zindler and Hart (1986). Red circles (table 1) and star symbols (data from Khodami and Davoudian 2008) show the late Miocene–Pliocene volcanic rocks from the south-east of Isfahan, and white circles are from the north-west of Isfahan (data from Khodami 2011).

4. Discussion

4.1 *Geochemistry*

According to the geochemical studies of Khodami *et al.* (2010), the rocks have SiO_2 content ranging from 55.73 to 65.63 wt% and these are medium to high K calc-alkaline and meta-aluminous. The rocks show a composition from andesite to dacite in total alkali against a silica diagram (figure 3) (Khodami *et al.* 2010). Furthermore, parts of the volcanic rocks have adakitic characteristics (Khodami *et al.* 2009). The chondrite-normalised rare-earth element (REE) patterns show light rare-earth element (LREE) enrichment and heavy rare-earth element (HREE) depletion without (europium) Eu anomaly (figure 4a). The primitive mantle-normalised multi-element diagram is characterised by the enrichment of large ion lithophile elements (LILEs) (Rb, Ba, K, Sr and especially Pb) and depletion in high field-strength elements (HFSEs) (Nb, Ta, P and Ti) (figure 4b) (Khodami *et al.* 2009, 2010). The negative Nb, Ta and Ti anomalies are indicative of subduction origin (Zhang *et al.* 2007). The enrichment of Sr without Eu anomaly and the depletion of HREE and Y suggest the absence of plagioclase and the existence of garnet as a residue in the source, respectively (Khodami *et al.* 2009, 2010). Slab-derived fluids and melts resulted in the enrichment of LILE and alkali elements. However, more preferential enrichment of Rb rather than that of K occurs (Zhang *et al.* 2007), and the HFSE (Nb, Ta, P and Ti) prefer to remain in phases such as rutile, ilmenite or amphibole by source (Pearce 1983; Wilson 1989). The rocks in the area have low contents of Nb/U (1.74–5) and Ce/Pb (0.47–4.03) (Khodami *et al.* 2009, 2010). The low Nb/U ratios display mantle metasomatism (Zhang *et al.* 2007). Also, the proportion of Ce as LREE to Pb as LILE is related to the special extraction of Pb from slab to mantle wedge, indicating more of the influence of subducted sediments (White 2003; Qian *et al.* 2016). The variations of La/Yb ratios against Yb show heterogeneity in the source region (figure 5a). Furthermore, Ba/Th *vs.* La/Sm, Th/La *vs.* Ce/Pb and Ba/La *vs.* Th/Yb diagrams indicate the involvement of slab-derived melts in the mantle source (figure 5b–d) (Wang *et al.* 2006; Arslan *et al.* 2013; Qian *et al.* 2016). In addition, the La/Nb *vs.* Th/Nb diagram can discriminate MORB–ocean island basalt (OIB) and three main crustal inputs: subduction, contamination with continental crust and crustal recycling during delamination (Pearce 2008). The subducted sediment averages are dispersed above the MORB–OIB array. The samples are plotted above the MORB–OIB array and scattered in the field of subducted sediments from the different subduction settings (figure 6). These geochemical features show that slab-derived melts and fluids are recycled into the mantle source.

4.2 *Isotope features*

The volcanic rocks show limited variations in Pb, Sr and Nd isotopic compositions with $^{206}Pb/^{204}Pb = 18.41–18.72$; $^{207}Pb/^{204}Pb = 15.64–15.67$; $^{208}Pb/^{204}Pb = 38.49–38.83$; $^{207}Pb/^{206}Pb = 0.8372–0.8496$; $^{208}Pb/^{206}Pb = 2.0743–2.0905$; $^{87}Sr/^{86}Sr = 0.7051–0.7068$ and $^{143}Nd/^{144}Nd = 0.5125$. The rocks also have a $\Delta 7/4Pb$ range of 15.44–15.82 and a $\Delta 8/4Pb$ range of 57.26–60.44 (table 1). As mentioned above, the geochemical features suggested an enrichment mantle source. Also, based on the isotopic ratios of Pb, Sr and Nd, major and trace elements, the origin of magma and the role of crustal components have been studied. Crustal contamination results in a significant increase in $^{87}Sr/^{86}Sr$ ratios and a positive correlation with SiO_2 (Wang *et al.* 2006; Gao *et al.* 2007) but this correlation is not observed for the $^{87}Sr/^{86}Sr$ *vs.* SiO_2 diagram for the volcanic rocks in the area (figure 7a). Moreover, the Sr isotope ratios are plotted against the magmatic differentiation index (MDI) and show metasomatism at source (figure 7b). Both diagrams show that magma escaped from contamination by crustal components during magma ascension and composition variations of the rocks have been controlled by metasomatism processes at source.

Moreover, the $^{87}Sr/^{86}Sr$ ratio in the rocks is higher than MORB and DMM, showing the addition of more radiogenic Sr to the mantle source (Lustrino and Anderson 2015). The volcanic rocks plot in the mantle array towards the EMII in the $^{143}Nd/^{144}Nd$ *vs.* $^{87}Sr/^{86}Sr$ diagram (figure 8a). The rocks have a high isotopic composition of Sr and Pb compared to DMM and EMI, and their isotopic composition is scattered towards the EMII in the $^{206}Pb/^{204}Pb$ *vs.* $^{87}Sr/^{86}Sr$ diagram (figure 8b). Nevertheless, the $^{87}Sr/^{86}Sr$ ratio shows amounts lower than the EMII. The volcanic rocks have $^{206}Pb/^{204}Pb$ and $^{207}Pb/^{204}Pb$ ratios more than the EMI, DMM and the lower continental crust, and a $^{208}Pb/^{204}Pb$ ratio higher than the DMM. Despite the small number of analyses, the data are well ranged in the Pb isotopes diagram

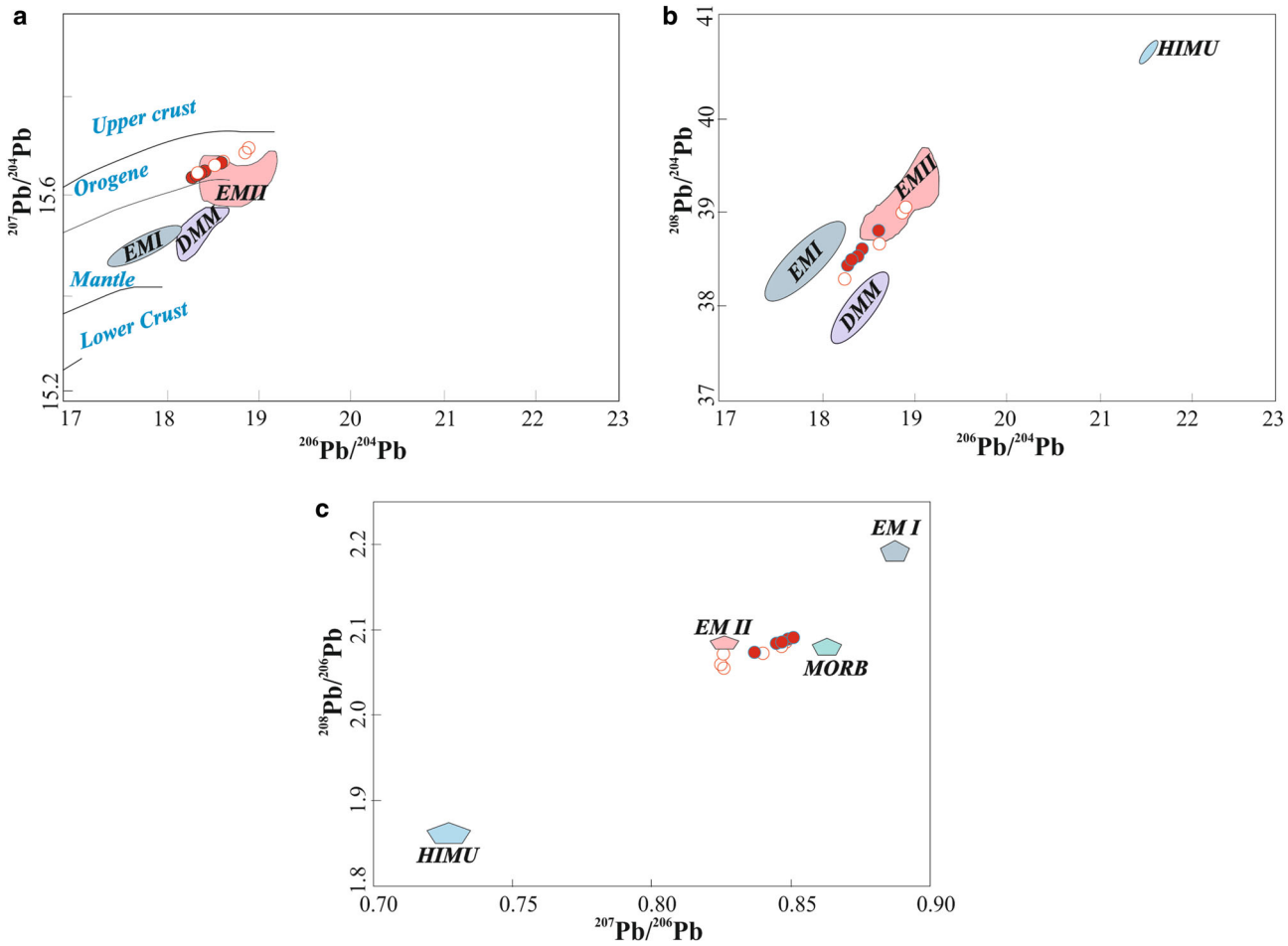

Figure 9. Plots of Pb isotopic ratios for the volcanic rocks: (**a**) $^{207}Pb/^{204}Pb$ *vs.* $^{206}Pb/^{204}Pb$ diagram. (**b**) $^{208}Pb/^{204}Pb$ *vs.* $^{206}Pb/^{204}Pb$ diagram. (**c**) $^{208}Pb/^{206}Pb$ *vs.* $^{207}Pb/^{206}Pb$ diagram. Mantle reservoir including depleted mantle (DM), enriched mantle I (EMI), enriched mantle II (EMII) and high U/Pb mantle (HIMU) are from Zindler and Hart (1986) Reference lines after Zartman and Doe (1981). MORB data are from Mukasa *et al.* (1994) and Pb isotope ratios in main terrestrial reservoirs are from White (2003) (symbols are the same as those used in figure 8).

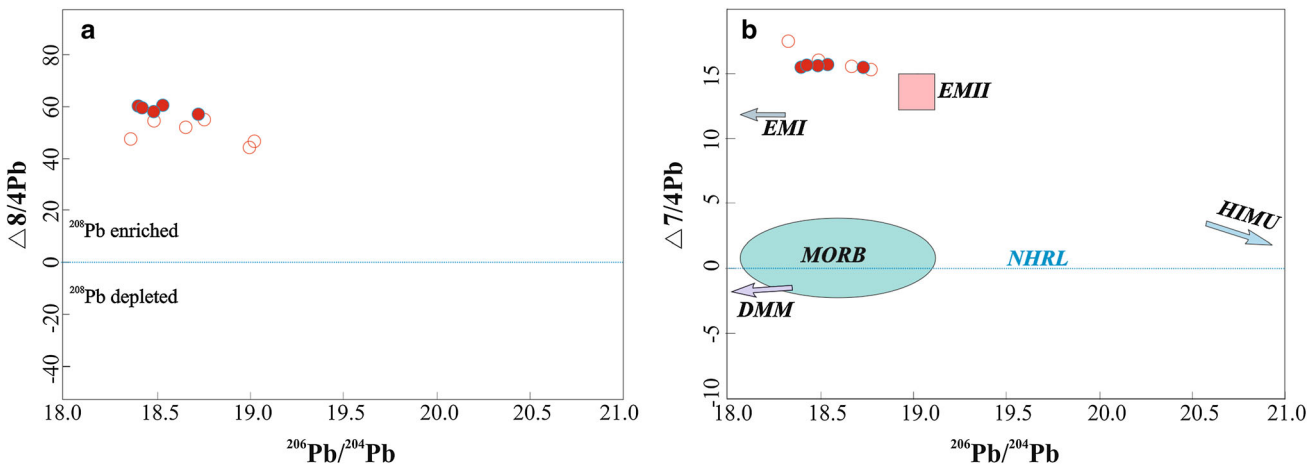

Figure 10. (**a**) Δ8/4 Pb *vs.* $^{206}Pb/^{204}Pb$ diagram. (**b**) Δ7/4 Pb *vs.* $^{206}Pb/^{204}Pb$ diagram (Arslan *et al.* 2013). The mantle reservoirs identified by Zindler and Hart (1986) and Hofman (1997); northern hemisphere reference line (NHRL) from Hart (1984) (symbols are the same as those used in figure 8).

and plotted near the EMII field (figures 8 and 9). Thoroughly in the $^{207}Pb/^{204}Pb$ *vs.* $^{206}Pb/^{204}Pb$, $^{208}Pb/^{204}Pb$ *vs.* $^{206}Pb/^{204}Pb$ and $^{208}Pb/^{206}Pb$ *vs.* $^{207}Pb/^{206}Pb$ diagrams, the volcanic rocks are plotted in the EMII or scattered towards the EMII field (figure 9a–c). Moreover, they are formed in the orogenic setting (figure 9a). The volcanic rocks have high amounts of radiogenic Pb ratios, positive Δ7/4 and Δ8/4 Pb, and plots above the north hemisphere reference line (NHRL) (figure 10a and b). The Δ8/4Pb values indicate high Th/U ratios, enrichment of radiogenic ^{208}Pb and probably the involvement of the crustal components in the source (Arslan *et al.* 2013). Also, the high $^{207}Pb/^{204}Pb$ ratios suggest the addition of more radiogenic Pb components to the source of magma. The $^{207}Pb/^{204}Pb$ ratio in the crust is more than that in the mantle and this ratio is sensitive to crustal components enrichment (Workman *et al.* 2004; Wang *et al.* 2006; Ge *et al.* 2015). The values of $^{208}Pb/^{204}Pb$ and $^{207}Pb/^{204}Pb$ *vs.* $^{206}Pb/^{204}Pb$ of volcanic rocks display enrichment by crust materials such as marine sediments or continental crust (figure 11a and b) (Arslan *et al.* 2013). Oceanic crust has high U and Th contents compared to the mantle due to their pelagic and terrigenous sediments (Wilson 1989; White 2003; Lustrino and Anderson 2015). As mentioned above, EMI and EMII are produced when pelagic (i.e., deep sea) and terrigenous (i.e., continental) sediments accompanied by slab are subducted in the mantle wedge and modified mantle. The Pb-isotope data are comparable to marine sediments such as those of the Atlantic and Indian oceans (figure 11c) (White 2003). The rate of mantle metasomatism is related to the composition of the slab and the degree of alteration and proportion of pelagic to terrigenous sediments (Workman *et al.* 2004; Lustrino and Anderson 2015). EMII type was created by the subduction of the oceanic crust and their terrigenous sediments comparable to the upper crust (Zindler and Hart 1986; Zhang *et al.* 2007). Thus, the marine sediments have a significant influence on the variation of isotopic ratios and geochemical features in the subduction environment. The oceanic crust and continental-derived sediments (terrigenous sediments) were recycled into the mantle wedge. Then, the enrichment of incompatible elements and the evolution of Pb isotopic ratios occurred in the mantle wedge. Pb is concentrated in phases such as feldspars and clays, while Sr is concentrated in carbonate-rich

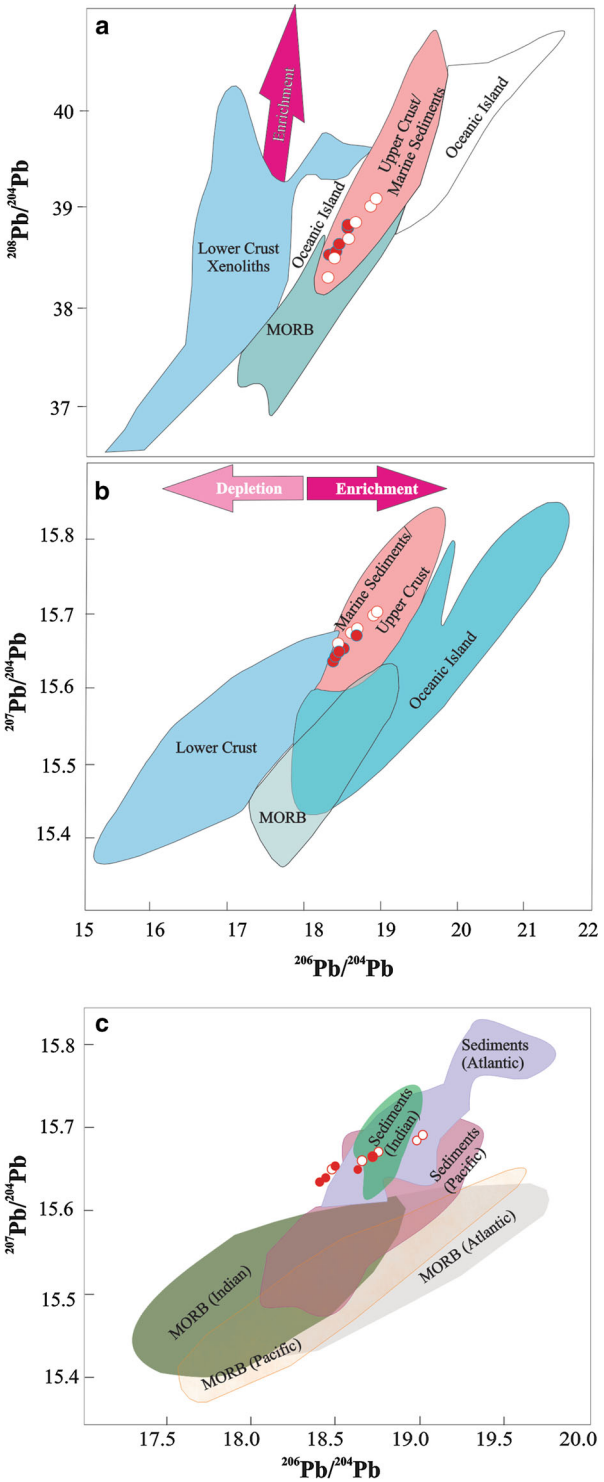

Figure 11. Plots of Pb isotopic ratios of volcanic rocks (Arslan *et al.* 2013): (**a**) $^{208}Pb/^{204}Pb$ *vs.* $^{206}Pb/^{204}Pb$ diagram. (**b**) $^{207}Pb/^{204}Pb$ *vs.* $^{206}Pb/^{204}Pb$ diagram. The mantle reservoirs were identified by Zindler and Hart (1986). Pb isotopic ratios in the major terrestrial reservoirs are from White (2003). (**c**) $^{207}Pb/^{204}Pb$ *vs.* $^{206}Pb/^{204}Pb$ diagram, showing data from the studied area compared with the Atlantic, Pacific and Indian MORB and marine sediments from Atlantic, Pacific and Indian oceans (White 2003) (symbols are the same as those used in figure 8).

sediments (White 2003), which is reflected in the isotopic composition of magma in the metasomatised mantle. Nevertheless, the amounts of Sr and Nd could remain in the range of mantle composition that is interpreted by the inadequacy in time for the Sr radiogenic evolution in the source or marine sediments composition (Mukasa *et al.* 1994; White 2003). Furthermore, Sr, Nd and Pb isotopic and geochemical data do not support the assimilation of crustal materials in the magma source for the volcanic rocks. Evidence also suggests the rapid ascent of magma. The calc-alkaline and related adakitic rocks from Tudeshk, the central part of the UDMA, show the partial melting of the enriched mantle source. Thus, it is possible that some adakitic volcanic rocks in UDMA are derived from a metasomatised mantle wedge (Azizi *et al.* 2014).

5. Conclusion

The late Miocene–Pliocene volcanic rocks in the south-east of Isfahan show mainly calc-alkaline to adakitic trends with relatively high LILE and LREE and low HFSE abundances. Depletion in the Nb, Ta and Ti and the Nb/La, Nb/U, La/Yb, Ba/Th, La/Sm, Th/Yb, Th/La, Ba/La and Ce/Pb ratios indicate heterogeneity in the mantle source. Sr, Nd and Pb isotopic ratios and whole-rock geochemical data from the late Miocene–Pliocene volcanic rocks in the south-east of Isfahan present new results with regard to the generation of post-collisional volcanism in UDMA. The results are as follows:

1. The studied volcanic rocks have a narrow range of $^{87}Sr/^{86}Sr$ (0.7051–0.7068) $^{143}Nd/^{144}Nd$ (0.5125) and Pb isotopic compositions ($^{206}Pb/^{204}Pb$ = 18.41–18.72, $^{207}Pb/^{204}Pb$ = 15.64–15.67, $^{208}Pb/^{204}Pb$ = 38.49–38.83), which demonstrate an enrichment mantle source.
2. The correlation between some elements and isotopes shows that crustal assimilation did not play a significant role in the geochemical and isotopic variation of the volcanic rocks.
3. Sr, Nd and Pb isotopic data suggest the involvement of EM-like mantle sources. The lower $^{143}Nd/^{144}Nd$, higher $^{87}Sr/^{86}Sr$, $^{207}Pb/^{204}Pb$ and $^{208}Pb/^{204}Pb$ than MORB are very similar to the EMII-type that need an additional subducted sediments involvement. Oceanic crust and terrigenous sediments were recycled into the mantle wedge and resulted in the enrichment of incompatible elements and the evolution of Pb isotopic ratios.
4. The late Miocene–Pliocene calc-alkaline and adakitic magma from Todeshk, south-east of Isfahan could be produced with an enriched mantle source. In this case, the role of the EMII has dominated over the other mantle end-members. The origin of the EMII involves the metasomatism of the mantle lithosphere, followed by the subduction and recycling of continental sediments related to the slab.

Acknowledgements

The author would like to thank Yazd University for the support and Dr Nahid Shabanian and the anonymous reviewers for the constructive comments which greatly contributed to the improvement of the paper.

References

Alavi M 1980 Tectonostratigraphic evolution of Zagrosides of Iran; *Geology* **8** 144–149.

Alavi M 1994 Tectonics of Zagros orogenic belt of Iran, new data and interpretation; *Tectonophys.* **229** 211–238.

Alavi M 2004 Regional stratigraphy of the Zagros Fold-Thrust belt of Iran and its proforeland evolution; *Am. J. Sci.* **304** 1–20.

Arslan M, Temizel I, Abdioglu E, Kolayli H, Yucel C, Boztug D and Sen C 2013 $^{40}Ar–^{39}Ar$ dating, whole-rock and Sr–Nd–Pb isotope geochemistry of post-collisional eocene volcanic rocks in the southern part of the eastern pontides (NE Turkey): Implications for magma evolution in extension-induced origin; *Contrib. Mineral. Petrol.* **166** 113–142.

Azizi H, Tsuboi Y M, Takemura K and Razyani S 2014 The role of heterogenetic mantle in the genesis of Adakites Northeast of Sanandaj, Northwestern Iran; *Chemie der Erde* **74** 87–97.

Berberian F and Berberian M 1981 Tectono-plutonic episodes in Iran; In: *Zagros, Hindukosh, Himalaya, geodynamic evolution* (eds) Gupta H K and Delany F M, American Geophysical Union, Washington DC, pp. 5–32.

Cox K G, Bell J D and Pankhurst R J 1979 *The interpretation of igneous rocks*; Unwin Hyman, London, 450p.

Davoudian A R, Genser J, Neubauer F and Shabanian N 2016 $^{40}Ar/^{39}Ar$ mineral ages of eclogites from North Shahrekord in the Sanandaj–Sirjan Zone, Iran: Implications for the tectonic evolution of Zagros orogeny; *Gondwana Res.* **37** 216–240.

Faure G 1986 *Principles of isotope geology* (2nd edn); Wiley, New York.

Gao Y, Hou Z, Kamber B S, Wei R, Meng X and Zhao R 2007 Adakite-like porphyries from the southern Tibetan continental collision zones: Evidence for slab melt metasomatism; *Contrib. Mineral. Petrol.* **153** 105–120.

Ge S, Zhai M, Safonova I, Li D, Zhu M, Zuo P and Shan H 2015 Whole-rock geochemistry and Sr–Nd–Pb isotope systematics of the late carboniferous volcanic rocks of the awulale metallogenic belt in the western Tianshan Mountains (NW China): Petrogenesis and geodynamical; *Lithos* **229** 62–77.

Ghasemi A and Talbot C J 2005 A new tectonic scenario for the Sanandaj–Sirjan Zone (Iran); *J. Asian Earth Sci.* **26** 683–693.

Ghorbani M, Graham I T and Ghaderi M 2014 Oligocene–miocene geodynamic evolution of the central part of Urumieh–Dokhtar Arc of Iran; *Int. Geol. Rev.* **56**(**8**) 1039–1050.

Hart S R 1984 A large-scale isotope anomaly in the southern hemisphere mantle; *Nature* **309** 753–757.

Hassanzadeh J 1993 Metallogenic and tectonomagmatic events in the SE sector of the Cenozoic active continental margin of Iran (Shahre Babak area, Kerman Province). PhD thesis, University of California, Los Angeles, 204p.

Hofman A W 1997 Mantle geochemistry: The message from oceanic volcanism; *Nature* **385** 219–229.

Khodami M 2011 Isotopic studies on volcanic rocks of Joushaghan–Kamu (Isfahan Province); The Report of Research Project, Islamic Azad University, Mahallat Branch (in Persian).

Khodami M and Davoudian A R 2008 Sr–Nd isotopic characteristics of neogene volcanic rocks in Southeast of Isfahan; In: *6th Swiss Geoscience Meeting*, Lugano, pp. 88–89.

Khodami M, Noghreyan M and Davoudian A R 2009 Pliocene–Quaternary Adakite volcanism in the Isfahan area, Central Iranian magmatic belt; *N. Jb. Miner. Abh.* **186**(**3**) 235–248.

Khodami M, Noghreyan M and Davoudian A R 2010 Geochemical constraints on the genesis of the volcanic rocks in the Southeast of Isfahan Area, Iran; *Arab. J. Geosci.* **3** 257–266.

Lustrino M and Anderson D L 2015 The mantle isotopic printer: Basic mantle plume geochemistry for seismologists and geodynamicists; In: *The interdisciplinary earth, chapter* 16 (eds) Foulger G R, Lustrino M and King S D, The Geological Society of America, Special Paper 514 and *Am. Geophys. Union Spec. Publ.* **71** 257–279.

Mohajjel M, Fergusson C L and Sahandi M R 2003 Cretaceous–Tertiary convergence and continental collision, Sanandaj–Sirjan zone, western Iran; *J. Asian Earth Sci.* **21** 397–412.

Mukasa S B, Flower M F J and Miklius A 1994 The Nd–Sr and Pb-isotopic character of lavas from taal, Laguna De Bay and arayat volcanoes, southwestern luzon, Philippines: Implications for Arc magma petrogenesis; *Tectonophys.* **235** 205–221.

Nabavi M and Amidi M 1978 Geological map of Nain 1:250000, Geological Survey of Iran.

Nakamura N 1974 Determination of REE, Ba, Fe, Mg, Na and K in carbonaceous and ordinary chondrites; *Geochim. Cosmochim. Acta* **38** 757–775.

Omrani J, Agard P, Whitechurch H, Benoit M, Prouteau G and Jolivet L 2008 Arc-magmatism and subduction history beneath the Zagros mountains, Iran: A new report of adakites and geodynamic consequences; *Lithos* **106** 380–398.

Pearce J A 1983 Role of the sub-continental lithosphere in magma genesis at active continental margins; In: *Continental basalts and mantle xenoliths* (eds) Hawkesworth C J, Norry M J and Shiva, Cheshire, UK, pp. 230–249.

Pearce J A 2008 Geochemical fingerprinting of oceanic basalts with applications to ophiolite classification and the search for Archean oceanic crust; *Lithos* **100** 14–48.

Plank T and Langmuir C H 1998 The chemical composition of subducting sediment and its consequences for the crust and mantle; *Chem. Geol.* **145** 325–394.

Qian X, Wang Y, Feng Q, Zi J, Zhang Y and Chonglakmani Ch 2016 Petrogenesis and tectonic implication of the late triassic post-collisional volcanic rocks in Chiang Khong, NW Thailand; *Lithos* **248** 418–431.

Rudnick R L and Fountain D M 1995 Nature and composition of the continental crust-a lower crustal perspective; *Rev. Geophys.* **33** 267–309.

Stöcklin J 1968 Structural history and tectonics of Iran: A review; *Am. Assoc. Petrol. Geol. Bull.* **52** 1229–1258.

Sun S and Mcdonough W F 1989 Chemical and isotopic systematic of oceanic basalts: Implication for mantle composition and processes; In: *Magmatism in the ocean basins* (eds) Saunders A D and Norry M J, *Geol. Soc. London,* pp. 313–345.

Tatsumi Y and Takahashi T 2006 Operation of subduction factory and production of andesite; *J. Miner. Petrol. Sci.* **101** 145–153.

Wang P J, Chen F, Chen S M, Siebel W and Satir M 2006 Geochemical and Nd–Sr–Pb isotopic composition of mesozoic volcanic rocks in the songliao basin. NE China; *Geochem. J.* **40** 149–159.

White W M 2003 *Geochemistry*; Cambridge University Press, London, 339p.

Wilson M 1989 *Igneous petrogenesis. A global tectonic approach*; Unwin Hyman, London, 466p.

Workman R K, Hart S R, Jackson M, Regelous M, Farley K A, Blusztajn J, Kurz M and Staudigel H 2004 Recycled metasomatized lithosphere as the origin of the enriched mantle II (EMII) End-member: Evidence from the samoan volcanic chain; *Geochem. Geophys. Geosyst.* **5** 1–44.

Yamgouot F N, Déruelle B, Gbambié I B, Ngounouno M I and Demaiffe D 2016 Geochemistry of the volcanic rocks from bioko island (Cameroon Hot line): Evidence for plume-lithosphere interaction; *Geosci. Frontiers* **7** 743–757.

Zartman R E and Doe B R 1981 Plumbotectonics – the model; *Tectonophys.* **75** 135–162.

Zhang Z, Xiao X, Wang J, Wang Y and Kusky T M 2007 Post-collisional plio–pleistocene shoshonitic volcanism in the western Kunlun mountains, NW China, geochemical constraints on mantle source characteristics and petrogenesis; *J. Asian Earth Sci.* **31**(**4**) 379–403.

Zindler A and Hart S R 1986 Chemical geodynamics; *Annu. Rev. Earth Pl. Sci.* **14** 493–571.

Corresponding editor: Rajneesh Bhutani